J Comput Aided Mol Des
DOI 10.1007/s10822-015-9881-0

Insights into resistance mechanism of the macrolide biosensor protein MphR(A) binding to macrolide antibiotic erythromycin by molecular dynamics simulation

Tingting Feng[1,2] · Yanjun Zhang[1] · Jing-Na Ding[1] · Song Fan[2] · Ju-Guang Han[1]

Received: 6 August 2015 / Accepted: 6 November 2015

Abstract Macrolide biosensor protein MphR(A) has been known as a key regulatory protein in metabolite sensing and genetic expression regulating. MphR(A) protein binds to macrolide antibiotic erythromycin (Ery) and releases the gene operon, thus activates expression of the mphA gene and initiates Ery resistance. The two mutant amino acid residues (V66L and V126L) might potentially disrupt Ery binding to MphR(A). In these studies, the binding of macrolide antibiotic Ery to wild type (Wt) MphR(A) and double mutant (V66L/V126L) MphR(A) are explored by molecular dynamics simulations. Compared to the Apo-MphR(A) protein and Wt-MphR(A)–Ery complex, many interesting effects owing to the double mutant (V66L/V126L) are discovered. In the case of Ery, Helix I which plays an important role in transcription shows itself a right-hand α helix in Wt-MphR(A)–Ery, whereas the activated helix is broken down in double mutant-V66L/V126L-MphR(A)–Ery. The calculated results exhibit that the double mutant V66L/V126L reduces the binding affinity of the V66L/V126L-MphR(A) to Ery, resulting in the block of Ery resistance. The binding free energy decomposition analysis reveals that the decrease of the binding affinity for the variant V66L/V126L-MphR(A)–Ery is mainly attributed to the gas phase electrostatic energies. The residue Leu66, Thr154, and Arg122 enhance the binding affinity of V66L/V126L-MphR(A) to Ery. The residues Tyr103 and His147 contributes mainly to binding energies in the Wt-MphR(A)–Ery complex, whereas the two residues have no contribution to the binding free energy inV66L/V126L-MphR(A)–Ery complex. Our study gives useful insights into the nature of amino acids mutation effect, the mechanism of blocking drug resistance at the atomic level and the characteristics in binding affinity for Ery to double mutant (V66L/V126L) MphR(A), which will contribute to the design of more effective macrolide antibiotics.

Keywords Macrolide biosensor protein · MphR(A) · Macrolide antibiotic · Resistance mechanism · Double mutant (V66L/V126L)

Introduction

Antibiotic resistance is a momentous global health threat nowadays, largely due to the misuse of antibiotic drugs [1]. It leads to less effective or failed treatment by current drugs and the rapid expansion of drug-resistant infections, which dramatically give impact on mortality and increase hospitalization costs [2].

Macrolide biosensor protein MphR(A) has been known a key regulatory protein in metabolite sensing and regulation of genetic expression [3]. Macrolide antibiotics include the natural product Erythromycin, and its derivatives, such as Azithromycin, and Clarithromycin. These drugs are active mainly against gram-positive bacteria [4, 5], and widely used for bacterial infections nowadays [6]. Resistance to these macrolide antibiotics is an important problem for the issue of human health [7]. Based on the studies in the past, these antibiotics can be controlled by various different mechanisms, such as drug target modification and the activation of efflux pumps [8, 9]. In bacteria cells, another primary

✉ Ju-Guang Han
jghan@ustc.edu.cn

[1] National Synchrotron Radiation Laboratory, University of Science and Technology of China, Hefei 230029, People's Republic of China

[2] College of Basic Medical Sciences of Anhui Medical University, Hefei 230024, People's Republic of China

Published online: 13 November 2015

strategy is the direct modification of these drugs by macrolide 2′-phosphotransferase I[Mph(A)], which is encoded by the mphA gene [10]. A natural macrolide antibiotic Ery binds to the protein MphR(A), which activates expression of the mphA gene and ultimately initiates Ery resistance [11, 12]. MphA inactivates Ery by phosphorylation of the 2′-hydroxyl group on the desosamine sugar, which can block downstream signaling pathways of Ery [11]. It has been shown that the expression of this resistance gene mphA is controlled at the transcriptional level by the protein, MphR(A) [6]. Bacterial cells carrying the mph(A) and mrx genes show high-level resistance to Ery. The mph(A), mrx, and mphR(A) genes exist as a gene cluster beginning with the mph(A) gene [11]. It is demonstrated that the transcription of gene cluster is negatively regulated by the protein MphR(A) [13]. Also, it has been reported that the transcription of mph(A)–mrx–mphR(A) gene cluster is blocked without Ery but activated by the combination of Ery and the protein MphR(A) [6]. Thus, bacteria harboring this gene cluster have the ability to "sense" the presence of Ery through protein MphR(A). The gene cluster is transcribed in the same direction with an apparent organization so that the protein MphR(A) represses its own expression in a negative feedback loop (Fig. 1). Bacterial cells govern the resistance to macrolide antibiotics by the MphR(A) protein. Ery binding to the protein MphR(A) causes release of the PmphR promoter and then activates expression of 2'-phosphotransferase Mph(A), inducing Ery resistance [14].

Therefore, to block the binding activity of Ery on MphR(A) is the means of effective treatment of bacterial drug resistance. The two mutant amino acid residues (V66L and V126L) might potentially disrupt Ery binding [6]. Hence, we are engaged in the study on resistance mechanism of the macrolide biosensor protein MphR(A) binding to macrolide antibiotic Ery by molecular dynamics (MD) simulation, which will help block negative feedback mechanism, and further block the drug resistance, finally bring the antibiotics into the powerful curative effect. Based on the structure of protein MphR(A) and the results of molecular dynamic simulations, we will give useful clues of optimization and synthesis of novel macrolide antibiotics.

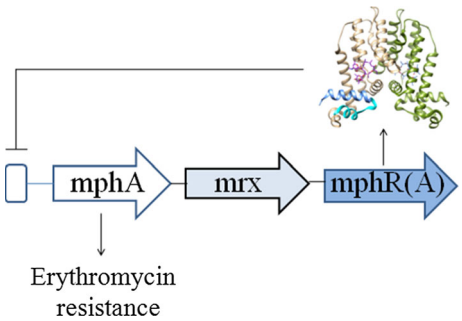

Fig. 1 Organization of the erythromycin resistance gene cassette. MphA is an erythromycin 2′-phosphotransferase

Material and computational method

Construction for the dynamical model

The protein dynamical models from the structure (PDB ID: 3FRQ) are adapted in the MD simulations [6]. The chemical structure of Ery is shown in Fig. 2a. The molecular Ery binding site is shown in Fig. 2b, c. For the sake of getting the most stable conformation and the electrostatic potential distributions, we calculated single point energies at the HF/6-31G(d,p) level by Gaussian 09 program [15].

Molecular dynamics simulations

For MD simulations, the complex protein wild-type (Wt) MphR(A) and the protein double mutant (V66L/V126L) MphR(A) with Ery structures were performed by using the AMBER12 program [16, 17]. The complex Wt-MphR(A)–Ery structure is adopted from the structure (PDB ID: 3FRQ) [6]. The double mutant (V66L/V126L) MphR(A)–Ery structure was obtained from the wild-type structure by modeling. The Apo-protein [wild-type (Wt) MphR(A)] system was acquired from the protein structure (PDB ID: 3G56), which does not bind the small molecule Ery [6]. The AMBER ff99SB force field parameters were adopted for the MD simulations [18, 19]. We added the missing hydrogen atoms of the proteins and Ery by LEaP module [20, 21]. The protein 3D model structures were solvated in the truncated octahedron periodic TIP3P water molecule box with the cutoff distance of 10 Å. We added an appropriate number of Na^+ counterions in order to neutralize the negative charge of each dynamic simulation system [17]. Finally, the structure Wt-MphR(A)-Apo contained 75950 atoms, V66L/V126L-Wt-MphR(A)–Ery contained 57219 atoms, and Wt-MphR(A)–Ery system was consist of 57618 atoms. We performed minimization steps for getting the initial dynamic simulation structures. Initially, the system was minimized by restraining all heavy atoms with a 500 kcal/(mol $Å^2$) strength. The entire system was optimized by 2500 cycles of steepest descent minimization and followed by 2500 cycles of conjugate gradient method. The next step, all restrains were removed, 5000 cycles of steepest descent method and 5000 cycles of conjugate gradient minimization were performed. After energy minimization, each simulation system was gradually heated from 0 to 300 K in increments of 25 ps with a 2 fs time step at a constant temperature of 300 K and then equilibrated at a constant pressure of 1 atm for another 25 ps. During MD simulations, we applied the Particle

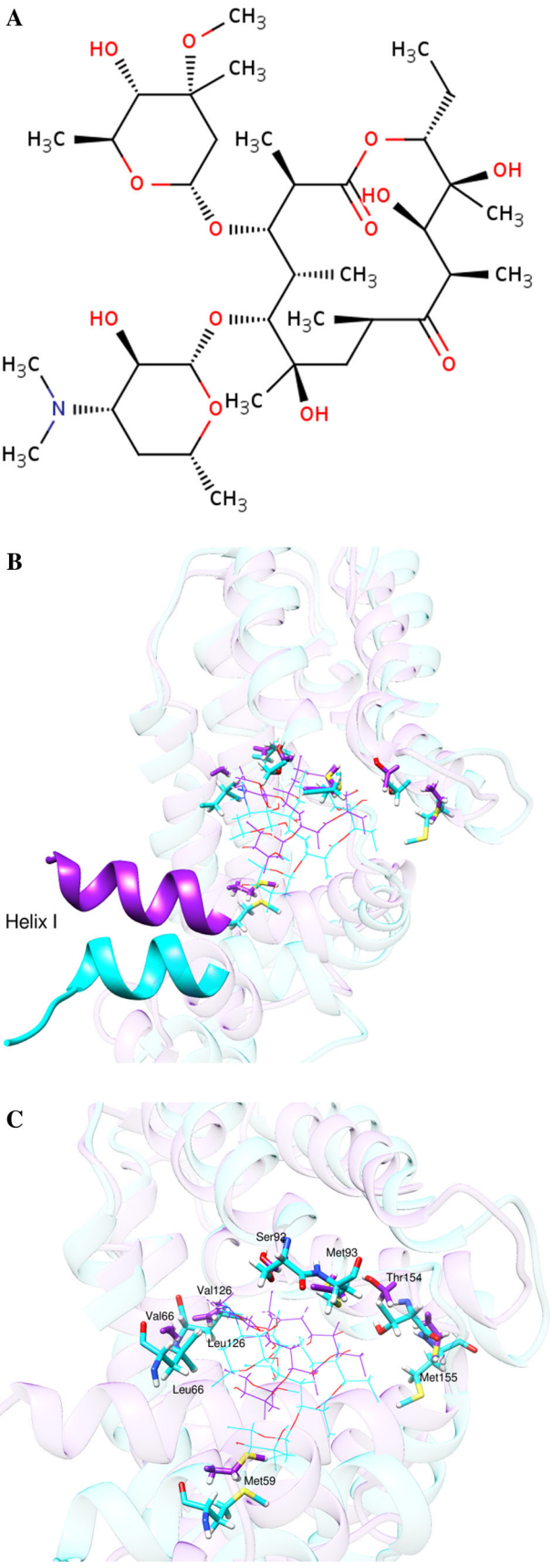

◀**Fig. 2** **a** Structure of Erythromycin. **b** the positions of Helix I in the Wt-MphR(A)–Ery, V66L/V126L-MphR(A)–Ery structures. Helix I in Wt-MphR(A) protein is shown as a purple ribbon. Helix I in V66L/V126L-MphR(A) is shown in cyan ribbon. **c** the relative positions of the mutations and the ligand binding site: the residues in Wt-MphR(A) complex is shown in purple ribbon, the ligand is shown in purple wire, the residues in V66L/V126L-MphR(A)–Ery-complex is shown in cyan ribbon, the ligand is shown in cyan wire; the residues in the ligand binding site are shown in stick model

Mesh Ewald (PME) to calculate long-rang electrostatics energies [22]. The SHAKE algorithm method was employed to restrict bonds containing hydrogen atoms [23]. All MD simulations was 2 fs time step performed by PMEMD module, and the coordinate files were saved at intervals of 2 ps for the analysis by PTRAJ module [16, 22]. We adopted the PROPKA program and H++ server to assign the protonation states of residues of the MD models [24]. Figures were accomplished with the Chimera1.9 program.

The binding free energy calculation

The MM-GB/SA methods were adopted for the calculation of the binding free energies. The GB model was performed in the AMBER12 program calculation [25]. For each MD simulation system (Wt-MphR(A)–Ery and V66L/V126L-MphR(A)–Ery), 1000 snapshots were extracted from the last 25 ns MD trajectory with an interval of 25 ps. The binding free energy (ΔG_{bind}) of Ery to the protein MphR(A) were calculated by the follow equations:

$$\Delta G_{bind} = G_{complex} - (G_{receptor} + G_{ligand} \quad (1)$$

Here $G_{complex}$, $G_{receptor}$ and G_{ligand} express the binding free energies of the complex, receptor (protein), and the ligand (Ery) in the solvent systems, respectively.

In Eq. (1), each binding free energy parameter comprises the molecular mechanics energy (ΔE_{MM}), the solvent energy (ΔG_{gol}) and the gas phase conformational thermodynamics entropy effect to the binding ($T\Delta S$). The binding free energy is calculated as follows:

$$\Delta\Delta G_{TOT} = \Delta E_{MM} + \Delta G_{gol} - T\Delta S \quad (2)$$

where the molecular mechanics free energy ΔE_{MM} is split into electrostatic interactions ΔE_{ele} and van der Waals interactions ΔE_{vdw} in the gas phase, it can be expressed as:

$$\Delta E_{MM} = \Delta E_{ele} + \Delta E_{vdw} \quad (3)$$

The solvation free energy (ΔG_{gol}) can be divided into two terms, the polar (ΔG_{GB}) and nonpolar contributions (ΔG_{SA}). The equation is expressed as:

$$\Delta G_{gol} = \Delta G_{GB} + \Delta G_{SA} \quad (4)$$

The ΔG_{gol} was computed with the AMBER12 suite GB module (IGB = 2). The dielectric constant was set to 1.0 inside the solute and 80.0 for the solvent. The nonpolar solvation free energy (ΔG_{SA}) was computed as follows:

$$G_{SA} = \gamma \times SASA + \beta \quad (5)$$

where SASA was estimated by the MSMS algorithm with a solvent probe radius value of 1.4 Å. The empirical constants γ and β were 0.0072 kcal/(mol Å2) and 0.0, respectively.

The solute entropy contributions (TΔS) were calculated by a normal mode analysis (NMA) with the NMODE module [17, 26]. For the system which contains many amino acids, the calculation of the solute entropy was so time-consuming that we took 100 snapshots from the final 25 ns equilibrium trajectory of each dynamic system for the conformational thermodynamics entropy calculations.

Results

RMSD analysis

To explore the effect of the small molecule Ery on the conformational stability of the protein MphR(A) and double mutant (V66L/V126L)-MphR(A), RMSD values of the position differences of backbone atoms among Wt-MphR(A)-Apo, Wt-MphR(A)–Ery and V66L/V126L-MphR(A)–Ery systems were calculated throughout the MD simulations (Fig. 3). The proteins of Wt-MphR(A)–Ery and V66L/V126L-MphR(A)–Ery systems show similar deviations from their starting structures. For the structure of the Wt-MphR(A)-Apo the trajectory shows a rapid increase to 6.5 ± 0.20 Å after 30 ns of the simulation run, indicating an immediate departure from its starting structure. The larger RMSD values for Wt-MphR(A)-Apo structure indicate that the overall topologies of the structure has been changed [27]. In contrast, the Wt-MphR(A)–Ery and V66L/V126L-MphR(A)–Ery show smaller RMSD value or greater stability during the entire MD simulations with the overall topology similar to the starting structure. Thus, we can conclude that the binding of small molecule Ery can enhance the stability of the Wt-MphR(A) and V66L/V126L-MphR(A) proteins in the case of accessible conformations.

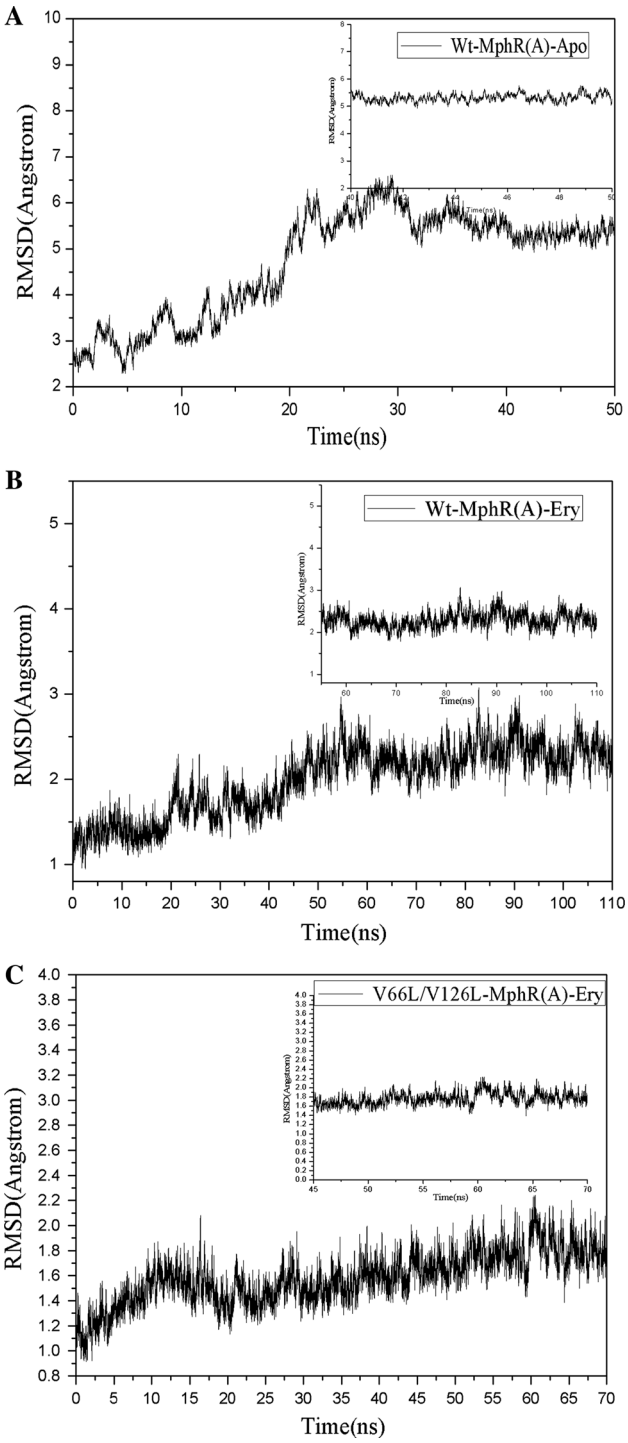

Fig. 3 The root-mean-square deviation (RMSD) of the backbone C_α atoms during the MD simulations of the complex with respect to the initial minimized structure of complex structures as a function of time

Radius of gyration

For the purpose of finding the MD mechanism of Ery binding to the protein MphR(A), we evaluate the compactness of the studied proteins. The size of protein is roughly estimated by radius of gyration (Rg), which is defined as the mass-weighted positional mean of the distances of atoms from the center of mass [28]. In the presence of Ery, the level of the compaction of MphR(A) and V66L/V126L-MphR(A) was determined by the radius of gyration (Rg) calculation becausethe Rg

describes the compaction level of the protein structure, the lower Rg indicates the more compactness of the protein. Figure 4 shows the most significant changes in Rg of the proteins, moreover, the change of the radius of gyration (Rg) of Wt-MphR(A)-Apo, V66L/V126L-MphR(A)–Ery, and Wt-MphR(A)–Ery has been measured. The average values of Rg are 23.51 ± 0.64 Å, 22.74 ± 0.70 Å, and 22.49 ± 0.81 Å for respective Wt-MphR(A)-Apo, V66L/V126L-MphR(A)–Ery, and Wt-MphR(A)–Ery. In comparison with Wt-MphR(A)-Apo system, V66L/V126L-MphR(A)–Ery, and Wt-MphR(A)–Ery systems show strongly structural stabilities indicated by the smaller Rg values(22.74 ± 0.70 Å and 22.49 ± 0.81 Å). The variation of Rg show that the protein compacted in V66L/V126L-MphR(A)–Ery and Wt-MphR(A)–Ery systems; and the protein MphR(A) has been expanded in Wt-MphR(A)-Apo system. According to the plots in Fig. 4, we can conclude that the protein MphR(A) is compacted when bound to the compound Ery.

Intrinsic and ligand-induced flexibility

The RMSF is considered as a fundamental parameter to expresses the mean fluctuation of the dynamical system residues/atoms [29]. The RMSF of each residue (Cα atoms) in the complexes [Wt-MphR(A)-Apo, V66L/V126L-MphR(A)–Ery, and Wt-MphR(A)–Ery] were calculated (Fig. 5). The high RMSF value indicates more flexibility while low RMSF value indicates the limited flexibility. As shown in Fig. 5, the fluctuations are stronger in the Wt-MphR(A)-Apo and V66L/V126L-MphR(A)–Ery systems. With Ery bound to Wt-MphR(A), RMSF plot of the residues has decreased. In order to determine whether the mutation affects the dynamic behavior of residues, the RMSF values of the three dynamic systems are compiled in Fig. 5. The fluctuation score clearly

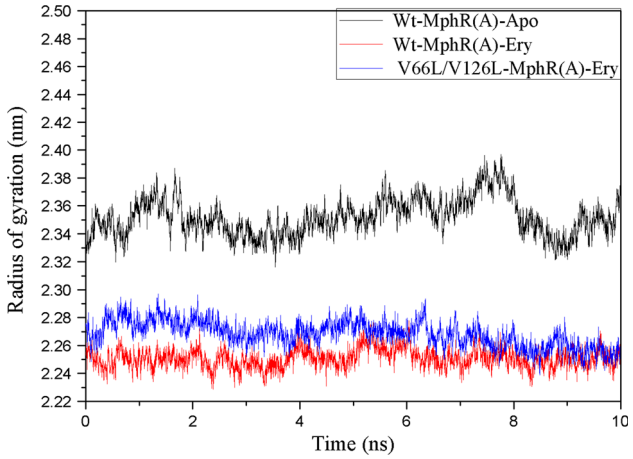

Fig. 4 The radius of gyration at the last 15 ns molecular simulation trajectories as a function of time

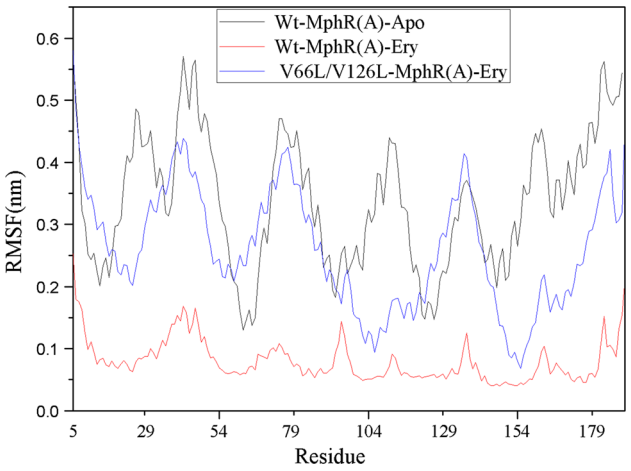

Fig. 5 The root-mean-square fluctuations (RMSF) of backbone atoms versus residue number of the Wt-MphR(A)-Apo, Wt-MphR(A)–Ery, V66L/V126L-MphR(A)–Ery structures

demonstrates an overall increase in the flexibility for V66L/V126L-MphR(A)–Ery as compared to Wt-MphR(A)- Ery. The increased RMSF not only affects the overall conformational fluctuation but also increases the fluctuation among active site residues, which plays a key role in the decreased Ery grip and the subsequent Ery resistance blocking-up. We can conclude that the V66L/V126L mutant heightens the protein flexibility and dynamics activities, which agree well with the binding free energy results below. Furthermore, we supposed that the V66L/V126L mutant might effect the interactions of protein-Ery by changing the secondary protein structure.

Structural transitions in helix I: folding into a right-handed α helix in Wt-MphR(A)–Ery complex

For the purpose of analyzing the protein secondary structure,we apply the Ramachandran Diagram which divide the two dimensions regions of φ-ψ space into several bins as described in Fig. 6. The distribution of the residues in the different bins is determined and the percentage values for each residue (Lys5-Asp10) are calculated. Figure 7 represents the percentage values distributed in Bins 1, 2, 8, and 9 regions for residues (Lys5-Asp10). The characterized regions of the φ-ψ space in Ramachandran Diagram are represented by Bin1 (β strand) and Bin9 (β strand), Bin 2 [polyproline II (PII)], Bin8 (right-handed α helix) [30]. Figure 6 (A) graphically illustrates the nature of residues(Lys5-Asp10) that have the propensity to lie in a specific region of φ-ψ space (Bin1-9). As shown in Fig. 6b, the residue Lys5 mainly distributed in Bin1 and Bin2 regions in the three systems. The residue Leu6 of Wt-MphR(A)-Apo has 54.04 % propensity to lie in Bin2, the same residue has 91.32 % propensity in Wt-MphR(A)–Ery

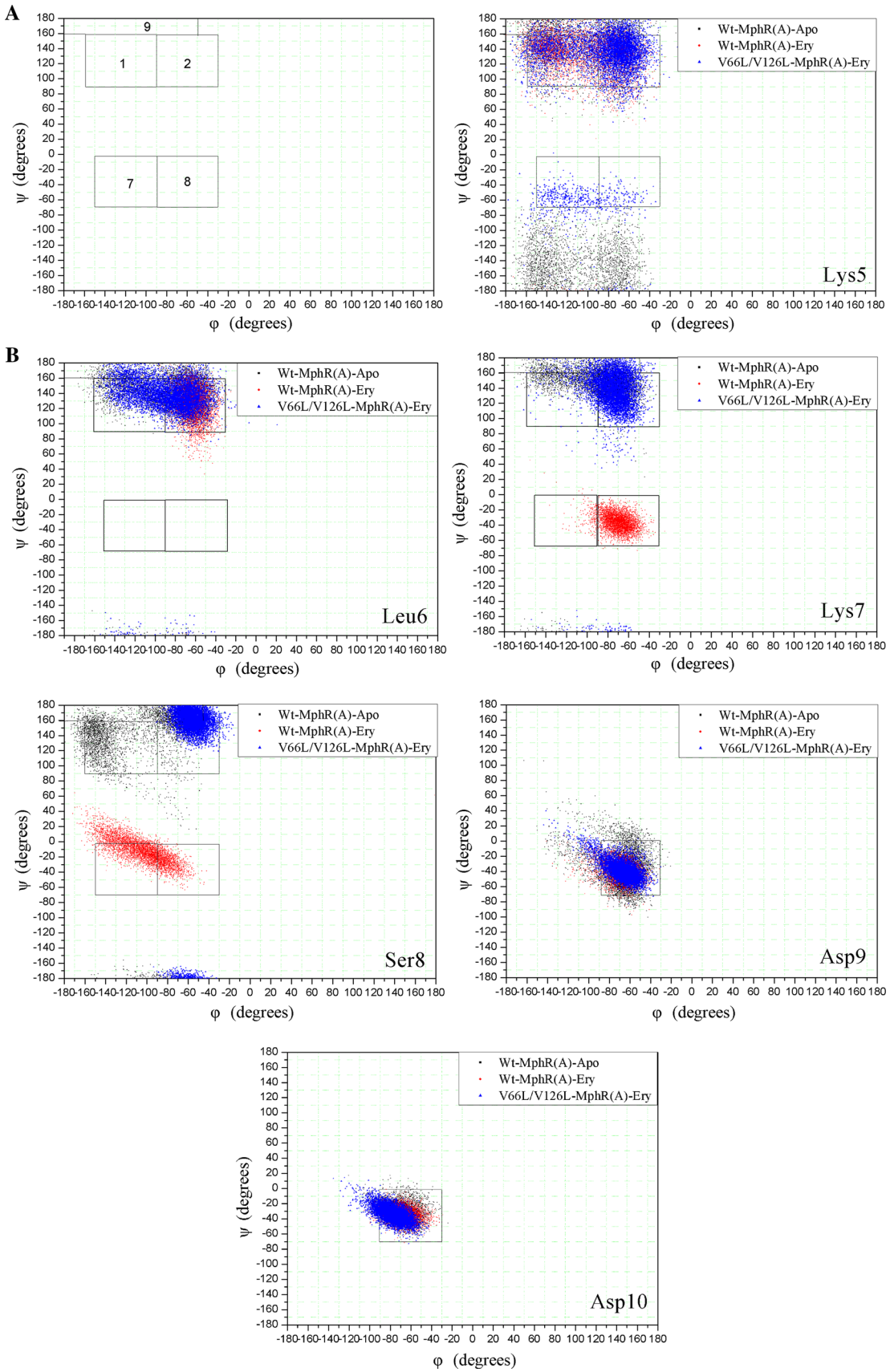
A
9
1
2
7
8
ψ (degrees)
φ (degrees)
Wt-MphR(A)-Apo
Wt-MphR(A)-Ery
V66L/V126L-MphR(A)-Ery
Lys5
B
Leu6
Lys7
Ser8
Asp9
Asp10

◀**Fig. 6** **a** Boundaries of the discrete bins are shown in the background of Ramachandran Map. **b** Scatter plot in φ-ψ space for residues (Lys5, Leu6, Lys7, Ser8, Asp9, and Asp10) are shown in the background of Ramachandran map

and 54.14 % propensity in V66L/V126L-MphR(A)–Ery. The residues (Lys7 and Ser8) of Wt-MphR(A)-Apo and V66L/V126L-MphR(A)–Ery mainly distributed in respective Bin9 and Bin2. Whereas the residue Lys7 of Wt-MphR(A)–Ery has 96.08 % propensity to lie in Bin8, Ser8 has 28.13 % propensity to lie in Bin8. The residue Asp9 and Asp10 mainly lie in Bin8 in the three systems. Bins 1, 2, and 9 represent residues in extended and semi-extended (PII) protein secondary conformations, whereas Bin8 represents residues in the strongly clustered α-helical conformation.

The data above indicated that the secondary structure of residue Lys7 has a significant change in the three systems, the residue Lys7 represents itself in extended and semi-extended (PII) conformations in Wt-MphR(A)-Apo and V66L/V126L-MphR(A)–Ery, but represents itself in a α-helical conformation in Wt-MphR(A)–Ery. This is an important discovery,it is reported that Helix I of the protein MphR(A) plays an important role in transcription [6]. Helix I domain of MphR(A) binds specifically to the promoter region of mph(A) [6, 11]. The structural transition in Helix I might affect the binding of the protein MphR(A) to the promoter of the mph(A) gene [31]. We will further focus on the molecular mechanism of the Ery resistance transformation resulting from the structural transitions in Helix I.

Distance in binding site cavity

To obtain the protein–ligand interactions, we calculated the average distance between the Cα of the key residue Met93 and Lys7 in Wt-MphR(A)-Apo, Wt-MphR(A)–Ery, and V66L/V126L-MphR(A)–Ery complex. The distance plots versus time are showed in Fig. 8a. The average distance between the Cα of the residue Lys7 and Cα of the residue Met93 in Wt-MphR(A)-Apo, Wt-MphR(A)–Ery, and V66L/V126L-MphR(A)–Ery are calculated to be 28.11 ± 0.80 Å, 23.71 ± 0.84 Å, and 27.45 ± 0.64 Å, respectively (Fig. 8b).

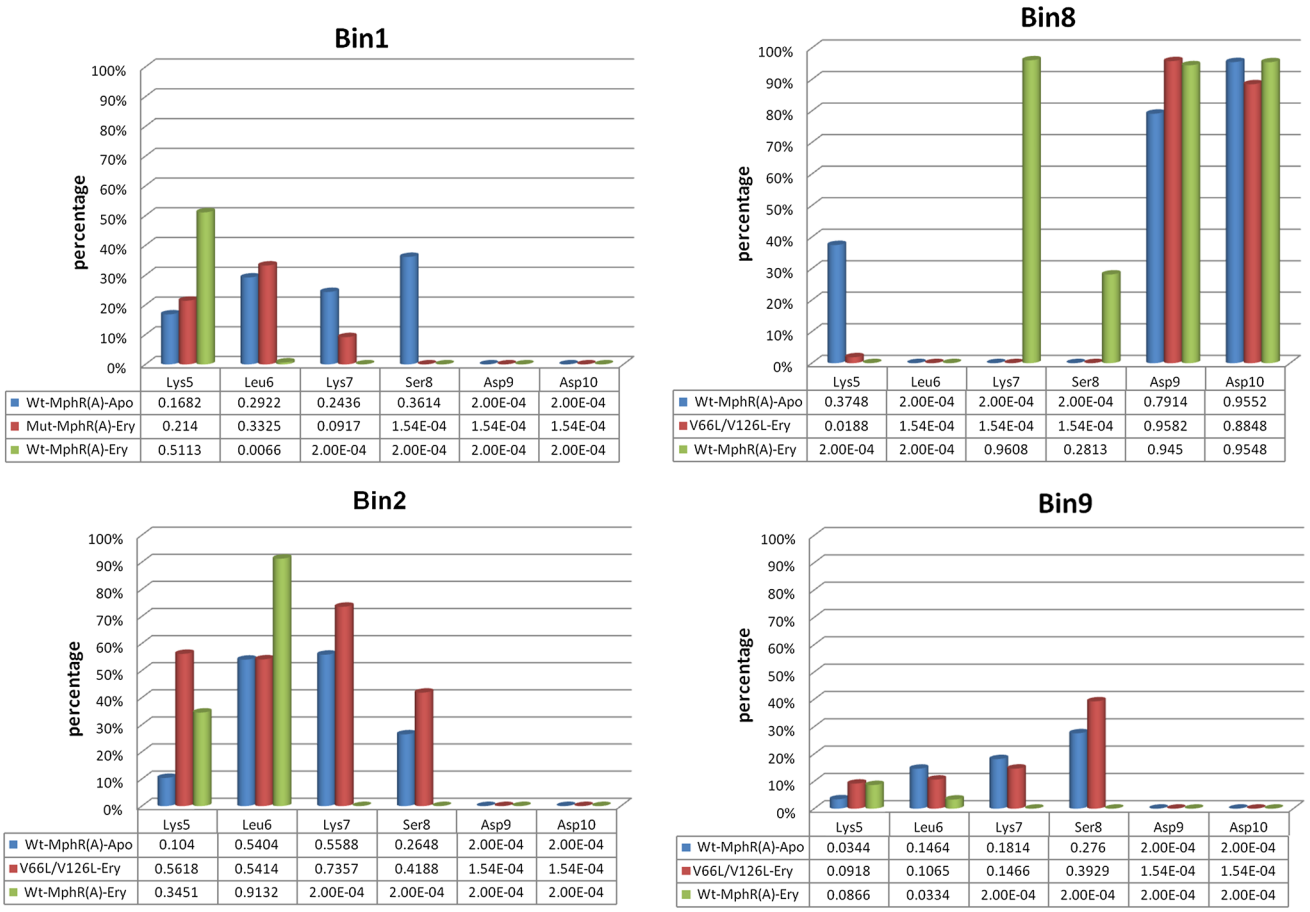

Fig. 7 percentages of the scatter in Bin1, Bin2, Bin8, and Bin9

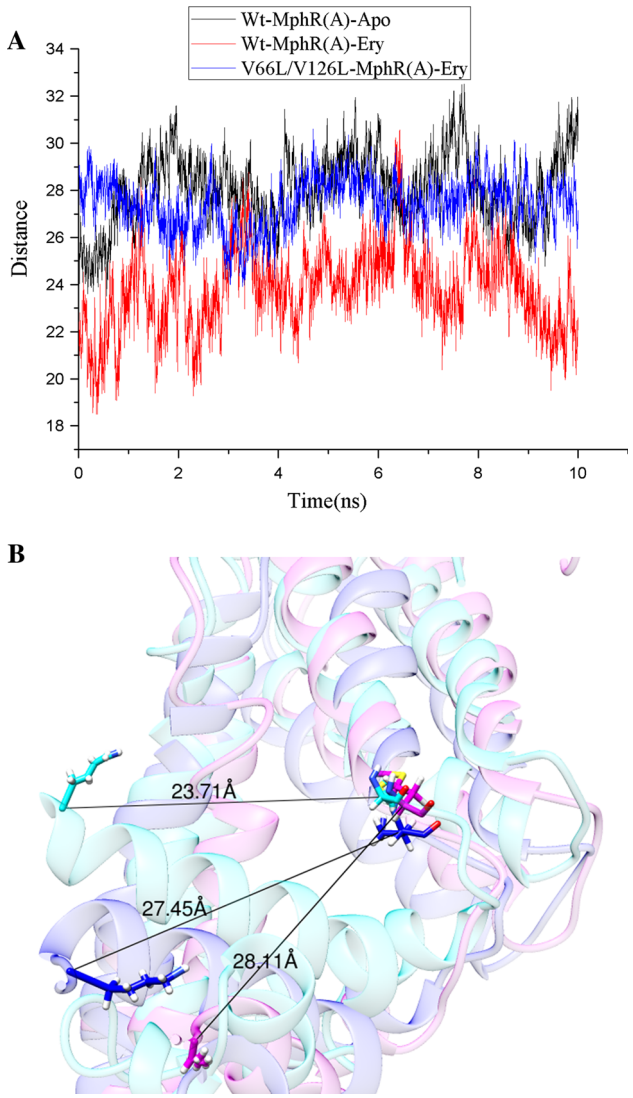

Fig. 8 **a** Variability of residue Met93 and Lys7' Cα distance. **b** Superposition of the chain A of the average structure of Wt-MphR(A)-Apo, Wt-MphR(A)–Ery, and V66L/V126L-MphR(A)–Ery from the last 10 ns molecular simulation trajectories according to RMSD. In the superimpositions, the protein residues are shown in ribbon and key residue Met93 and Lys in stick. The structures of Wt-MphR(A)–Ery, V66L/V126L-MphR(A)–Ery and Wt-MphR(A)-Apo, are colored with cyan, blue and magenta, respectively. The average distances between the Cα of the key residue Met93 and Lys7 in the three systems are labeled

The calculated results show that Ery fits properly and is accommodated well inside the binding site cavity in Wt-MphR(A)–Ery complex. Furthermore, the distance between the C_α of the residue Lys7 and the residue Met93 in V66L/V126L-MphR(A)–Ery is larger than that in Wt-MphR(A)–Ery, which might be a factor of the smaller binding free energy between Ery and V66L/V126L-MphR(A) in V66L/V126L-MphR(A)–Ery.

Binding free energy calculation

To insight to the binding free energy contribution spectrum of Ery with Wt-MphR(A) and double mutant V66L/V126L-MphR(A), absolute binding free energies are computed for the two systems by using the MM-GBSA methods [26]. The binding free energy contribution spectrum of Wt-MphR(A)–Ery and V66L/V126L-MphR(A)–Ery complexes are summarized in Table 1. As listed in Table 1, the total binding free energies of Wt-MphR(A)–Ery and V66L/V126L-MphR(A)–Ery complexes are −95.22 and −91.54 kcal/mol, respectively, which implies that the protein V66L/V126L-MphR(A) exhibits the weak binding affinity to Ery and the binding free energy of the V66L/V126L-MphR(A) to Ery is decreased by 3.68 kcal/mol in comparison with that of the Wt-MphR(A)–Ery complex. Moreover, the weakened binding affinity suggests that the mutated V66L/V126L-MphR(A) can not bind to Ery well. In addition, the calculated binding free energy results for Wt-MphR(A)–Ery and V66L/V126L-MphR(A)–Ery agree well with the available experimental affinities [6]. For the purpose of exploring the binding affinity contribution of each energy term, we analyze the individual energy terms and thermodynamic entropy effect (−TΔS) of the Wt-MphR(A)–Ery and V66L/V126L-MphR(A)–Ery complexes. Entropy (−TΔS) of Wt-MphR(A)–Ery is bigger than that of V66L/V126L-MphR(A)–Ery complex, Entropy (−TΔS) in the Wt-MphR(A)–Ery complex is 36.9 kcal/mol, while thermodynamic entropy value in the V66L/V126L-MphR(A)–Ery complex is 38.17 kcal/mol, displaying that the thermodynamic entropy effect in V66L/V126L-MphR(A)–Ery complex is not helpful for the binding; Finally, the absolute binding free energy of V66L/V126L-MphR(A)–Ery is −53.37 kcal/mol. For V66L/V126L-MphR(A)–Ery complex, the gas phase electrostatic energy (ΔE_{ele}) and van der Waals interaction(ΔE_{vdw}) are respective −50.1 and −150.48 kcal/mol, which give the major contributions to the binding. The nonpolar solvation energy (ΔG_{SA}) contributes −19.22 kcal/mol to Ery binding. On the contrary, the polar solvation energy (ΔG_{GB}) contributes 128.26 kcal/mol,which indicates that it is not favorable for Ery binding to the protein V66L/V126L-MphR(A). In the Wt-MphR(A)–Ery complex, the calculated protein-Ery binding free energy (ΔG_{bind}) is −58.32 kcal/mol, it is extremely helpful for the Ery binding to the protein Wt-MphR(A). As shown in the Table 1, electrostatic energy in the gas phase (ΔE_{ele}) and van der Waals energy (ΔE_{vdw}) (−83.53 and −155 kcal/mol) provide the primary favorable binding free energy contributions. The nonpolar solvation energy (ΔG_{SA}) is much smaller (−20.24 kcal/mol) and polar solvation energy (ΔG_{GB}) is 163.55 kcal/mol, indicating that it is not conducive to the Ery binding to the

Table 1 Binding Free Energies (kcal/mol) in each system

System	ΔE_{ele}	ΔE_{VDW}	ΔG_{GAS}	ΔG_{GA}	ΔG_{GB}	ΔGB_{SOL}	ΔGB_{ele}	ΔG_{bind}	$-T\Delta S$	$\Delta\Delta G_{TOT}$
V66L/V126L-MphR(A)–Ery	−50.1	−150.48	−200.58	−19.22	128.26	109.04	78.16	−91.54	38.17	−53.37
Wt-MphR(A)–Ery	−83.53	−155	−238.53	−20.24	163.55	143.31	80.03	−95.22	36.9	−58.32

Average contributions to the binding free energies in both erythromycin (Ery) bound systems calculate over the last 25 ns of each system MD trajectory corresponding to equilibrium. ΔE_{ele} and ΔE_{vdw} are the molecular mechanics electrostatic and van der Waals contributions; ΔG_{SA} is the polar component of the solvation free energy, whereas ΔG_{GB} is the nonpolar component. $T\Delta S$ is the entropic contribution. ΔG_{bind} is the total binding energy (calculated as the average of the individual $\Delta E_{ele} + \Delta E_{vdw} + \Delta G_{SA} + \Delta G_{GB}$ contributions for each MD snapshot); $\Delta G_{bind} = \Delta E_{ele} + \Delta E_{vdw} + \Delta G_{SA} + \Delta G_{GB}$; $\Delta\Delta G_{TOT} = \Delta E_{ele} + \Delta E_{vdw} + \Delta G_{SA} + \Delta G_{GB} - T\Delta S$

protein Wt-MphR(A). To insight into the differences in energetic contributions, we find that in the Wt-MphR(A)–Ery system, the residue Thr17, Tyr103 and His147 contribute −0.72, −1.44 and −1.84 kcal/mol, respectively. However, the three residues have no binding free energies in the V66L/V126L-MphR(A)–Ery complex. Meanwhile, in the V66L/V126L-MphR(A)–Ery, the mutant residues Leu66 and Leu126 have binding free energy contributions of −2.24 and −1.07 kcal/mol. In Wt-MphR(A)–Ery complex, the binding free energy contributions of the residues Val66 and Val126 are −1.09 and −0.84 kcal/mol, respectively.

Binding free energy decomposition analysis

To explore the contributions of binding free energy of each residue, the energies are decomposed into individual residue contributions by using the MM-GBSA method. The decomposition of energy contains molecular mechanics energy and solvation energy, but does not include entropy effects. We divide ΔG values into two terms: the net electrostatic energies ($\Delta E_{ele} + \Delta G_{GB}$) and the non-polar energies ($\Delta E_{vdw} + \Delta G_{SA}$) [32]. In order to understand effect of the variation of V66L/V126L-MphR(A) binding to Ery, the interaction of each residue and Ery can be calculated (Figs. 9, 10). For Wt-MphR(A)–Ery, the main energy contributors are the residue Met59, Val66, Ser92, Met93, Tyr103, Val126, His147, Thr154, and Met155. The main binding driving forces of the nine residues and Ery are van der Waals energies (ΔE_{vdw}) and the nonpolar solvation energies (ΔG_{SA}). In V66L/V126L-MphR(A)–Ery, main energy contribution residues are Met59, Leu66, Ser92, Met93, Arg122, Leu126, Thr154, and Met155. Except for the residue Thr154, the gas phase electrostatic interaction (ΔE_{ele}) and the polar solvation energy (ΔG_{GB}) play the main roles in the binding. The binding energy contribution of the other residues are mainly from van der Waals interaction (ΔE_{vdw}) and the nonpolar solvation energy (ΔG_{SA}) (Fig. 10). The total binding energy contributions of the eight residues are −2.24, −2.04, −1.52, −2.06, −2.51, −1.07, −2.82, and −1.35 kcal/mol, respectively. For V66L/V126L-MphR(A)–Ery complex, Thr154 is the most favorable residue for the binding free energy contribution, its total energy contribution is −2.82 kcal/mol, the net electrostatic energy ($\Delta E_{ele} + \Delta G_{GB}$) is −1.81 kcal/mol and the non-polar interaction ($\Delta E_{vdw} + \Delta G_{SA}$) is −1.01 kcal/mol. For Wt-MphR(A)–Ery system, the residues Met59, Val66, Ser92, Met93, Tyr103, Val126, His147, Thr154, and Met155 made large

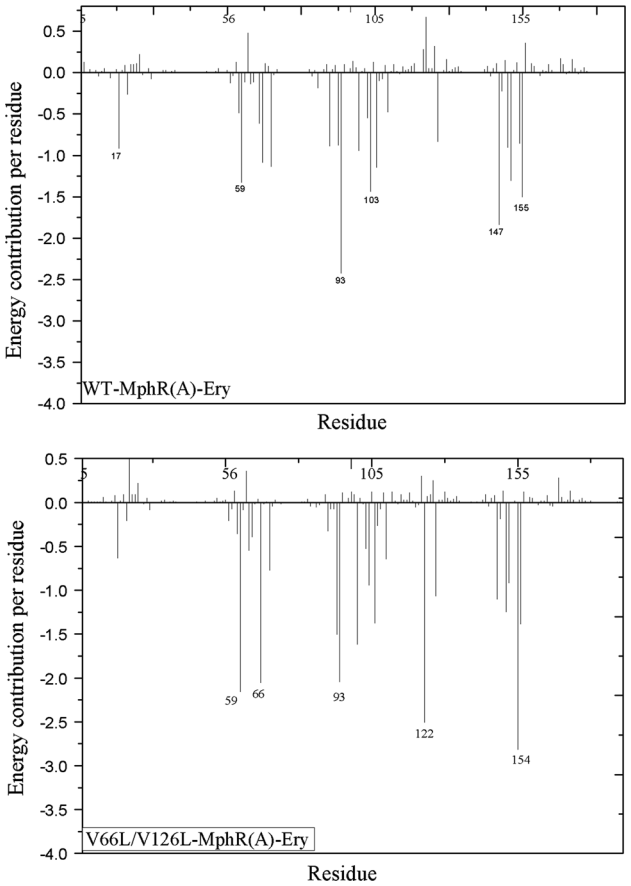

Fig. 9 Decomposition of binding free energy on per-residue basis for each complex

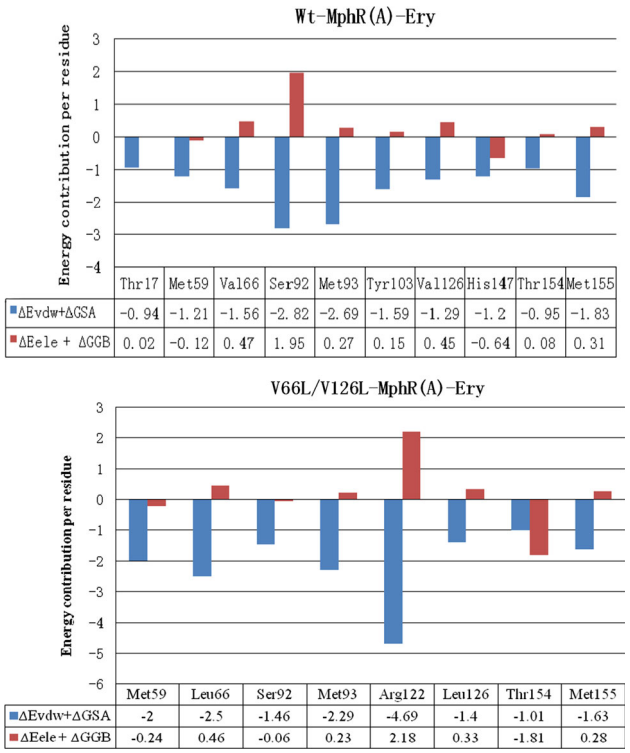

Fig. 10 Comparison of interaction energies based on the key residues in the complexes

contributions to Ery binding to the protein Wt-MphR(A). The total free energy contributions are −1.33, −1.09, −0.87, −2.42, −1.44, −0.84, −1.84, −0.87, and −1.52 kcal/mol, respectively. As shown in Fig. 10, Met93 makes a notable contribution to the binding free energy, its total energy contribution is −2.42 kcal/mol and net electrostatic energy ($\Delta E_{ele} + \Delta G_{GB}$) is 0.27 kcal/mol,the nonpolar energy ($\Delta E_{vdw} + \Delta G_{SA}$) is −2.69 kcal/mol.

H-bonds and binding mode analysis

For better visualizing and comparing the binding modes of Wt-MphR(A)–Ery and V66L/V126L-MphR(A)–Ery complex, the average structures of the two structures were extracted. In order to investigate the influence of the configuration from the hydrogen bonding network, hydrogen bond lengths and occupies were calculated by the PTRAJ module of AMBER12 during the MD simulations, and the results are listed in Table 2. Hydrogen bonding network is shown in Fig. 11. Hydrogen bonds were counted with the distance cutoff (3.5 Å between two heavy atoms) and angle cut off (120° among heavy atom -hydrogen -heavy atom). For the Wt-MphR(A)–Ery complex, the occupancy of hydrogen bonds formed between main chain carbonyl oxygen atom (O) of Ser92 and 3-hydroxy hydrogen atom (H40-O10) of Ery is 79.10 %. The occupancy of hydrogen bond formed between the side chain imidazolyl hydrogen atom (NE2-HE2) of His147 and xacyclotetradecane-2,10-dione oxygen atom(O2) of Ery is 93.80 %, this hydrogen bond plays very important role in the stability. The main chain carbonyl oxygen atom(O) of the residue Met58 and pyran hydrogen atom (H49-O13) of Ery form a hydrogen bond, its occupancy is 28.09 %, the occupancy of hydrogen bond is obviously reduced, resulting in the nearer distance of Met58 carbonyl oxygen atom(O) and Ery pyran oxygen atom(O13) and the two atoms are negatively charged, the electrostatic repulsive force heightens because of the nearer distance, which reduces the role of the hydrogen bond.

For the V66L/V126L-MphR(A)–Ery complex, the occupancy of the hydrogen bond formed between main chain carbonyl oxygen atom (O) of the residue Ser92 and 3-hydroxy hydrogen atom (H40-O10) of Ery is 85.45 %. The oxygen atom (OG) of Ser92 side chain oxhydryl is negatively charged and 3-hydroxy hydrogen atom (H40-O10) of Ery is positively charged, therefore,the larger electrostatic attraction exists between the two atoms. As the Table 3 shown, electrostatic interactions in the gas phase of Ser92 side chain are −1.4 kcal/mol. The hydrogen bond exists between the hydrogen atom (HE–NE) of Arg122 side chain guanidyl and xacyclotetradecane-2,10-dione oxygen atom(O3) of Ery, the occupancy is 34.40 %, the nitrogen atom of Arg122 side chain guanidyl and oxygen atom(O3) of Ery is nearer in distance and negatively charged, the existence of the electrostatic repulsion reduces the effect of the hydrogen bond. As the Table 2 listed, gas phase energy of Arg122 is −18.52 kcal/mol ($T_{ele} = -14.31$ kcal/mol; $T_{VDW} = -4.21$ kcal/mol), its total solvation energy is 16.01 kcal/mol ($T_{GB} = 16.49$ kal/mol, $T_{SA} = -0.48$ kcal/mol). Meanwhile, the oxygen atom (OG1) of Thr154 side chain oxhydryl and xacyclotetradecane-2,10-dione hydrogen atom (H21-O7) of Ery forms a stable hydrogen bond, surprisingly, its occupancy is 99.26 %, it is obvious that the H bond is especially important to the binding affinity. The gas phase electrostatic energy of Thr154 side chain is −2.78 kcal/mol and electrostatic energy in the gas phase of Ser92 side chain is −1.4 kcal/mol, which illustrates that electrostatic interaction is a key interaction in the two residues. Meanwhile, the residues Ser92 and Thr154 play important role in the hydrogen bond interaction.

Structure-binding affinity relationship analysis

We performed MD simulations to investigate resistance mechanism of macrolide antibiotic Ery against the macrolide biosensor protein MphR(A). In order to monitor RMSD changes in the two systems, the 70 and 110 ns MD simulations are performed for respective Wt-MphR(A)–Ery and V66L/V126L-MphR(A)–Ery complexes. RMSD

Table 2 Percentage of hydrogen bonds (>25 %) MD Simulations between the compound and the residues around the erythromycin (Ery)

Compound	Donor	Acceptor	Occupancy (%)	Distance (Å)	Angle (°)
Wt-MphR(A)–Ery	Ery@O2	His147@NE2–HE2	93.80	2.936 (0.16)	18.85 (10.02)
	Ser92@O	Ery@O10–H40	79.10	2.845 (0.16)	19.51 (8.03)
	Met58@O	Ery@O13–H49	28.09	2.900 (0.20)	20.15 (10.01)
V66L/V126L–Ery	Thr154@OG1	Ery@O7–H21	99.26	2.864 (0.16)	16.44 (7.34)
	Ser92@O	Ery@O10–H40	85.45	2.835 (0.10)	15.14 (6.69)
	Ery@O3	Arg122@NE–HE	34.40	2.990 (0.19)	15.23 (9.23)

For every system, the cut-off used for hydrogen bond distance and angle is 3.5 Å and 120°, respectively. The percent hydrogen bond occupancy that hydrogen bonds formed during the MD simulations is produced by the PTRAJ module of AMBER12. In addition, each hydrogen bond distance is measured between the heavy atom of donor and the heavy atom of acceptor

assesses the structure state of energy convergence by MM-GBSA calculation, RMSD and the structure state of energy convergence demonstrate that the simulations of taking a state from the last 25 ns equilibrium trajectory every 25 ps for the subsequent calculation are reasonable [25, 33]. Using the MM-GBSA method to calculate the binding free energy of the system, the calculation results agree well with the experimental results [6, 14]. In addition, the results of decomposition of free energy for the different energies illustrate that change of the enthalpy are larger than that of the entropy in the two systems. Residue energy decomposition shows that Ery binding to Wt-MphR(A) mainly result from the nine residues, Met59, Val66, Ser92, Met93, Tyr103, Val126, His147, Thr154, and Met155. Based on dynamics simulation of V66L/V126L-MphR(A)–Ery complex, we find that the binding affinity of the protein V66L/V126L-MphR(A) and Ery is decreased. Through the energy decomposition on each residue, we find that the binding modes of the residues Leu66, Tyr103, Arg122, His147, and Thr154 are very different from that of Wt-MphR(A)–Ery, especially the residue Arg122 in Wt-MphR(A)–Ery almost loses the binding capacity, whereas in V66L/V126L-MphR(A)–Ery, Arg122 has a bigger energy contribution among the main amino acid residues. According to the hydrogen bond results and Fig. 11c, the hydrogen atom (NH2) of Arg122 side chain guanidyl and xacyclotetradecane-2,10-dione oxygen atom(O3) of Ery form a H-bond, resulting in the side chain guanidyl is closer to oxygen atom(O3) in distance. In Wt-MphR(A)–Ery, ΔE_{ele} of side chain imidazolylthe in residue His147 contributes to the binding, whereas side chain imidazolyl of the His147 represents a almost 90 degree rotation in V66L/V126L-MphR(A)–Ery (see Fig. 11d), and ΔE_{ele} is reduced a lot due to the side chain. As shown in Fig. 11e, the oxygen atom (OG1) of Thr154 side chain oxhydryl is near to xacyclotetradecane-2,10-dione hydrogen atom (H21-O7) of Ery, ΔE_{ele} emerges and the H-bond forms. On the contrary, there is no H-bond in the residue of Wt-MphR(A)–Ery complex. As for V66L/V126L-MphR(A)–Ery complex, the residue Val66 is mutated into the residue Leu66, the side chain of Leu is longer than that of Val, which makes van der Waals (ΔE_{vdw}) of the Leu66 side chain increases apparently, hydrogen atom of residue Leu66 side chain and Ery pyran ring forms CH…. π. Except for the residue Thr154, for the other amino acids, van der Waals energy (ΔE_{vdw}) and nonpolar solvation energies (ΔG_{SA}) are the main contributors. In addition to the residue His147 contributing to −0.64 kcal/mol polar effort ($\Delta E_{ele} + \Delta G_{GB}$) in the Wt-MphR(A)–Ery, non-polar effort ($\Delta E_{vdw} + \Delta G_{SA}$) is the main contributorfor the other amino acids.

Conclusions

The double mutant V66L/V126L-MphR(A) binding to Ery exhibits different conformation and dynamic behavior, such as the higher flexibility of residues, the looser active pocket, the structural transition in Helix I. The results imply less drug resistance, which is further verified in the binding affinity of theV66L/V126L-MphR(A) and Ery in energetic calculations. On the basis of the structural energetic analysis, we can conclude that the direct effects by the decrease in electrostatic energies for the side chains in residues Thr154 and Arg122; and the increase in van der Waals interactions for residue Tyr103 and electrostatic energies for residue His147 mainly achieve the Ery resistance in the Wt-MphR(A)–Ery. However, for the mutant V66L/V126L-MphR(A), the decrease in the binding affinity is mainly attributed to nonpolar solvation energies and van der Waals interactions of residues Leu66 and Arg122. As for the macrolide antibiotics, the decrease of the binding affinity suggests that the mutant V66L/V126L-MphR(A) cannot be well adapted by Ery, which relieves the drug resistance. The effect of mutant in combination with several key amino acid residues (V66L/V126L) leads to the conformational changes of the protein MphR(A), ultimately changes the transcriptional activity of MphR(A),

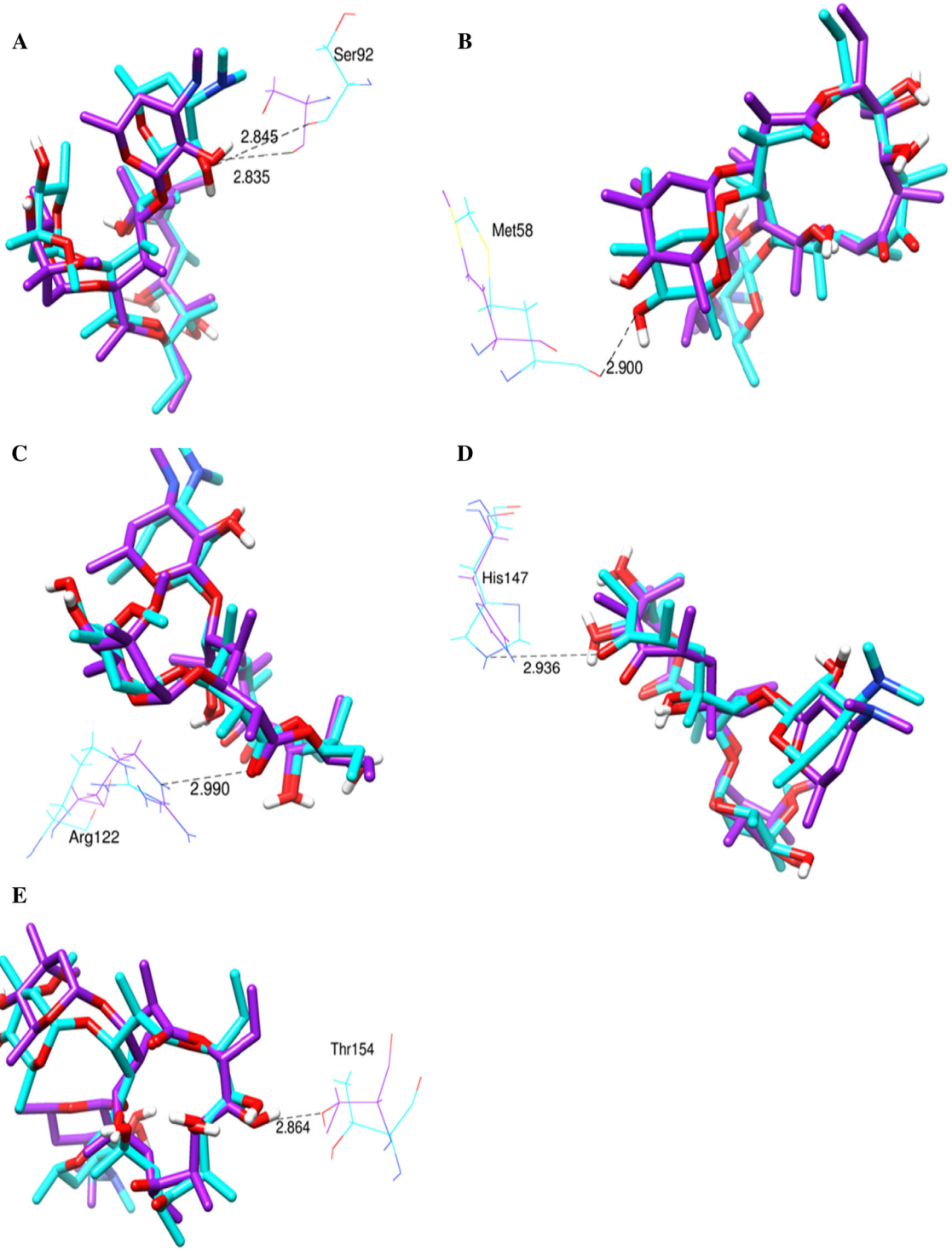

Fig. 11 H-bond interactions between the Ery and the residues (Ser92, Met58, Arg122, His147, Thr154). Ery in sticks is colored by the atom type, and residues are shown as wire (cyan, WT; purple, V66L/V126L). Superposition of average complex structures of Ery in Wt-MphR(A) and V66L/V126L-MphR(A) from the last 25 ns equilibrium trajectory, the Ery in Wt-MphR(A) complex is shown as a cyan stick model, hydrogen bonds are shown as dashed lines. The Ery in V66L/V126L-MphR(A)–Ery is shown in purple stick model. For clarity, the hydrogen atoms are omitted. The residues in Wt-MphR(A) complex is shown in cyan wire, the residues in V66L/V126L-MphR(A)–Ery-complex is shown in purple wire. The figure is created by using Chimera1.9 software

Table 3 Decomposition of ΔG (kcal/mol) on a per-residue basis (GB)

Residue	S_{VDW}	B_{VDW}	T_{VDW}	S_{ele}	Bele	T_{ele}	S_{GB}	B_{GB}	T_{GB}	T_{SA}	T_{GBTOT}
Wt–Ery											
Met58	−0.25	−0.28	−0.54	0.08	−0.24	−0.16	−0.04	0.3	0.26	−0.05	−0.49
Val66	−0.86	−0.53	−1.4	0.27	−0.35	−0.08	0.24	0.31	0.55	−0.16	−1.09
Ser92	−1.26	−1.22	−2.48	−0.42	−0.03	−0.45	1.15	1.26	2.4	−0.34	−0.87
Arg122	−2.96	−0.16	−3.12	0.25	−0.03	0.22	3.87	0.12	3.99	−0.42	0.67
Val126	−1.01	−0.13	−1.14	−0.11	−0.15	−0.25	0.44	0.26	0.7	−0.15	−0.84
His147	−0.78	−0.23	−1.01	−2.78	0.13	−2.64	2.13	−0.14	2	−0.19	−1.84
Thr154	−0.73	−0.15	−0.88	−0.47	−0.1	−0.57	0.48	0.17	0.65	−0.07	−0.87
V66L/V126L–Ery											
Met58	−0.26	−0.31	−0.57	0.01	0.02	0.03	0.05	0.2	0.25	−0.06	−0.36
Leu66	−1.57	−0.66	−2.23	−0.15	−0.31	−0.46	0.41	0.51	0.92	−0.27	−2.04
Ser92	−0.58	−0.6	−1.18	−1.4	0.23	−1.17	1.14	−0.03	1.11	−0.28	−1.52
Arg122	−3.92	−0.29	−4.21	−14.27	−0.04	−14.31	16.33	0.16	16.49	−0.48	−2.51
Leu126	−1.14	−0.1	−1.24	−0.33	−0.24	−0.57	0.48	0.43	0.9	−0.16	−1.07
His147	−0.8	−0.22	−1.02	−1.65	−0.11	−1.76	1.64	0.11	1.75	−0.07	−1.11
Thr154	−0.62	−0.3	−0.92	−2.87	0.09	−2.78	0.96	0.01	0.97	−0.09	−2.82

Energies shown as contributions from van der Waals energy (vdw), electrostatic energy (ele), polar solvation energy (GB), the nonpolar solvation energy (SA) of side chain atoms (S), backbone atoms (B), and the total (T) of protein -compound complex

and then effectively blocks macrolide antibiotic Ery resistance against the Macrolide biosensor protein MphR(A). We predict that our study can give useful insights into the nature of mutational effect, and the different characteristic in binding affinity of Ery and V66L/V126L-MphR(A). Further,we have docked the other macrolide antibiotics(Azithromycin, and Clarithromycin) into the ligand binding site of the protein MphR(A) and then perform MD simulations, these macrolide antibiotics have high binding affinities with the protein MphR(A). We focus on the structure-binding affinity relationships of these macrolide antibiotics, which will contribute to the design of more potent and effective macrolide antibiotics.

Acknowledgments The calculations of this paper were performed partly on the Supercomputing Center of University of Science and Technology of China.

References

1. Beatson SA, Walker MJ (2014) Tracking antibiotic resistance. Science 345(6203):1454–1455
2. Gopinath S et al (2014) Role of disease-associated tolerance in infectious superspreaders. Proc Natl Acad Sci USA 111(44): 15780–15785
3. Takakusagi K et al (2015) Multimodal biopanning of T7 phage-displayed peptides reveals angiomotin as a potential receptor of the anti-angiogenic macrolide Roxithromycin. Eur J Med Chem 90:809–821
4. Waters V, Ratjen F (2014) Antibiotic treatment for nontuberculous mycobacteria lung infection in people with cystic fibrosis. Cochrane Database Syst Rev (12):CD010004
5. Al-Taie O, Al-Taie E, Fischbach W (2014) Patients with Helicobacter pylori negative gastric marginal zone b-cell lymphoma (MZBCL) of MALT have a good prognosis. Z Gastroenterol 52(12):1389–1393
6. Zheng JT et al (2009) Structure and function of the macrolide biosensor protein, MphR(A), with and without erythromycin. J Mol Biol 387(5):1250–1260
7. Poor AE et al (2014) Control of multi-drug-resistant pathogens with non-thermal-plasma-treated alginate wound dressing. Surgical Infections 15(3):233–243
8. Szczepanowski R et al (2007) Novel macrolide resistance module carried by the IncP-1 beta resistance plasmid pRSB111, isolated from a wastewater treatment plant. Antimicrob Agents Chemother 51(2):673–678
9. Schumacher MA et al (2001) Structural mechanisms of QacR induction and multidrug recognition. Science 294(5549):2158–2163
10. Fuentes MAF et al (2014) Antimicrobial resistance determinants in antibiotic and biocide-resistant gram-negative bacteria from organic foods. Food Control 37:9–14
11. Marti E, Balcazar JL (2012) Multidrug resistance-encoding plasmid from Aeromonas sp strain P2G1. Clin Microbiol Infect 18(9):E366–E368
12. Kannan K, Vazquez-Laslop N, Mankin AS (2012) Selective protein synthesis by ribosomes with a drug-obstructed exit tunnel. Cell 151(3):508–520
13. Noguchi N et al (2000) Regulation of transcription of the mph(A) gene for macrolide 2′-phosphotransferase I in *Escherichia coli*: characterization of the regulatory gene mphR(A). J Bacteriol 182(18):5052–5058
14. Yu HY et al. (2011) Novel Regulator MphX represses activation of phenol hydroxylase genes caused by a XylR/DmpR-type regulator MphR in *Acinetobacter calcoaceticus*. Plos One 6(3):e17350
15. Petersson GA et al (2003) On the optimization of Gaussian basis sets. J Chem Phys 118(3):1101–1109
16. Kodchakorn K et al (2014) GPU accelerated molecular dynamics simulations for protein-protein interaction of ankyrin complex. Integr Ferroelectr 156(1):137–146

17. Case DA et al (2005) The Amber biomolecular simulation programs. J Comput Chem 26(16):1668–1688
18. Spasic A, Serafini J, Mathews DH (2012) The amber ff99 force field predicts relative free energy changes for RNA helix formation. J Chem Theory Comput 8(7):2497–2505
19. Li D et al (2014) Investigation on the mechanism for the binding and drug resistance of wild type and mutations of G86 residue in HIV-1 protease complexed with Darunavir by molecular dynamic simulation and free energy calculation. J Mol Model 20(2):2122
20. Nikitin AM, Milchevskiy YV, Lyubartsev AP (2014) A new AMBER-compatible force field parameter set for alkanes. J Mol Model 20(3):2143
21. Salomon-Ferrer R, Case DA, Walker RC (2013) An overview of the Amber biomolecular simulation package. Wiley Interdiscip Rev Comput Mol Sci 3(2):198–210
22. Steinbrecher T, Latzer J, Case DA (2012) Revised AMBER parameters for bioorganic phosphates. J Chem Theory Comput 8(11):4405–4412
23. Pearlman DA et al (1995) Amber, a package of computer-programs for applying molecular mechanics, normal-mode analysis, molecular-dynamics and free-energy calculations to simulate the structural and energetic properties of molecules. Comput Phys Commun 91(1–3):1–41
24. Simonson T, Carlsson J, Case DA (2004) Proton binding to proteins: pK(a) calculations with explicit and implicit solvent models. J Am Chem Soc 126(13):4167–4180
25. Greenidge PA et al (2013) MM/GBSA binding energy prediction on the PDBbind data set: successes, failures, and directions for further improvement. J Chem Inf Model 53(1):201–209
26. Godschalk F et al (2013) Comparison of MM/GBSA calculations based on explicit and implicit solvent simulations. Phys Chem Chem Phys 15(20):7731–7739
27. Singh MK, Dominy BN (2010) Thermodynamic resolution: how do errors in modeled protein structures affect binding affinity predictions? Proteins Struct Funct Bioinf 78(7):1613–1617
28. Deshmukh SA et al (2013) Atomistic insights into solvation dynamics and conformational transformation in thermo-sensitive and non-thermo-sensitive oligomers. Polymer 54(1):210–222
29. Pitera JW (2014) Expected distributions of root-mean-square positional deviations in proteins. J Phys Chem B 118(24): 6526–6530
30. Kalmankar NV, Ramakrishnan C, Balaram P (2014) Sparsely populated residue conformations in protein structures: revisiting "experimental" Ramachandran maps. Proteins Struct Funct Bioinf 82(7):1101–1112
31. Noguchi N et al (2000) Regulation of transcription of the mph(A) gene for macrolide 2'-phosphotransferase I in Escherichia coli: characterization of the regulatory gene mphR(A). J Bacteriol 182(18):5052–5058
32. Miller BR et al (2012) MMPBSA.py: an efficient program for end-state free energy calculations. J Chem Theory Comput 8(9):3314–3321
33. Sun HM, Hunter CA, Llamas EM (2015) The flexibility-complementarity dichotomy in receptor-ligand interactions. Chem Sci 6(2):1444–1453